Journal of Materials Chemistry A

Large-diameter and Heteroatom-doped Graphene Nanotubes Decorated with Transition Metals as Carbon Hosts for Lithium-Sulfur Batteries

Journal:	*Journal of Materials Chemistry A*
Manuscript ID	TA-ART-03-2019-002889.R1
Article Type:	Paper
Date Submitted by the Author:	08-May-2019
Complete List of Authors:	Ogoke, Ogechi ; University at Buffalo, SUNY, Chemical and Biological Engineering Hwang, Sooyeon; Brookhaven National Laboratory, Center for Functional Nanomaterials Hultman, Benjamin; University at Buffalo, SUNY, Chemical and Biological Engineering Chen, Mengjie; University at Buffalo, SUNY, Chemical and Biological Engineering Karakalos, Stavros; University of South Carolina, College of Engineering and Computing He, Yanghua; University at Buffalo, SUNY, Chemical and Biological Engineering Ramsey , Adam; University at Buffalo, SUNY, Chemical and Biological Engineering Su, Dong; Brookhaven National Laboratory, Center for Functional Nanomaterials Alexandridis, Paschalis; University at Buffalo - The State University of New York, Dept of Chemical & Biological Engineering Wu, Gang; University at Buffalo, SUNY, Chemical and Biological Engineering

Large-diameter and Heteroatom-doped Graphene Nanotubes Decorated with Transition Metals as Carbon Hosts for Lithium-Sulfur Batteries

Ogechi Ogoke[a,1], Sooyeon Hwang[b,1], Benjamin Hultman[a], Mengjie Chen[a,], Stavros Karakalos[c] Yanghua He[a], Adam Ramsey[a], Dong Su[b,*] ,Paschalis Alexandridis[a,*], and Gang Wu[a,*]

[a]Department of Chemical and Biological Engineering, University at Buffalo, The State University of New York, Buffalo, NY 14260, United States
Email: gangwu@buffalo.edu (G. Wu) and palexand@buffalo.edu (P. Alexandridis)

[b]Center for Functional Nanomaterials, Brookhaven National Laboratory, Upton, NY 11973, United States
Email: dsu@bnl.gov (D. Su)

[c]Department of Chemical Engineering, University of South Carolina, Columbia, SC 29208, United States

[1], These authors contributed equally

ABSTRACT

This work addresses performance issues of lithium sulfur (Li-S) batteries via retaining the polysulfide intermediates within a novel cathode nanocarbon host. Herein, we report a series of nitrogen and oxygen co-doped and transition metal-decorated large size (200-500 nm in dimeter) graphene nanotubes (M-GNTs) (M = Co, Ni, and/or Fe) as effective carbon hosts for sulfur cathodes (S@M-GNTs) in Li-S batteries. The exceptionally large diameters of the graphene tubes allow facile diffusion of sulfur inside the tubes with sufficient loadings yet leaving room for volume expansion during the lithiation process. The GNTs with the largest diameter and abundant N and O doping along with CoNiFe alloy decoration (FeCoNi-GNTs) exhibit the best sulfur cathode performance. In addition to the unique nanocarbon structures, the heteroatom dopants and transition metal nanoparticles likely also play promotional roles in retaining long-chain polysulfide discharge intermediates within the carbon host, therefore improving rate capability and cycle

stability. In particular, a S@FeCoNi-GNT cathode with a high sulfur loading (~4.5 mg-S cm^{-2}) exhibits discharge capacities up to 1234.7 mAh g^{-1} at C/20 and 909.0 mAh g^{-1} at C/5. A discharge capacity of 554.4 mAh g^{-1} at 1C after 500 cycles was retained, further demonstrating its encouraging potential in Li-S batteries.

Keywords: Carbon hosts, large size graphene tube, ultra-high sulfur loading, sulfur cathodes, Li-S batteries.

1. Introduction

Lithium-ion batteries (LIBs) currently take the leading role in energy storage technologies due to their reliable cyclic stability and reasonable energy density. Commercialized LIBs utilize $LiCoO_2$, $Li(Ni,Mn,Co)O_2$ or $LiFePO_4$ as cathode materials,[1, 2] which unfortunately are limiting factors for further improving energy storage density of LIBs. For example, $LiCoO_2$ has a relatively low theoretical capacity of 273 mAh g^{-1} that is further reduced to 140-150 mAh g^{-1} when the operation voltage is restricted to the 3.0 V- 4.2 V range.[3] Development of new cathode materials with higher theoretical capacities to replace $LiCoO_2$ and $LiFePO_4$ is crucial for advanced battery technologies. Sulfur is an environmentally friendly low cost material (-60-70$ per ton), therefore lithium sulfur batteries (Li-S) that encompass sulfur (S_8) as the active material in the cathode have been widely explored in last decade. The Li-S battery possesses a promising theoretical capacity of 1675 mAh g^{-1} and corresponding energy density of 2500 Wh kg^{-1},[4-8] therefore it has been considered as one of the leading candidates to replace oxide or phosphate cathode based LIBs.[9] While great progress has been made since 2009,[9-15] additional research is required to increase the cycle lifetime and rate capability of Li-S batteries. Li-S batteries typically rely on a carbon host, which counteracts the high electrical resistivity of the sulfur cathode. During battery reactions, various polysulfides Li_2S_x (x = 8, 6, 4, and 2) are produced as intermediate discharge products, and end with Li_2S as the fully

discharged product. Unfortunately, long-chain polysulfides (x = 8, 6, or 4) (LPS) are soluble in the liquid electrolyte, therefore causing a serious stability issue.[16] In addition, due to the solubility of LPS, a parasitic shuttling effect takes place during cycling where the soluble LPS migrate away from the cathode to the surface of the anode. Then they are reduced to lower order insoluble polysulfides (x = 2 or 1). This leads to the precipitation of polysulfides at the surface of the Li anode. During charging, the polysulfides deposited onto the anode migrate back to the cathode. This shuttling effect consumes a large number of electrons in internal side reactions, instead of generating desirable electrical current, which significantly reduces cycling efficiency, decreases the cycle lifetime, and increases self-discharge. Several tactics have been developed to retain the LPS within the S cathode including the use of a variety of carbon hosts,[17-30] physical encapsulation,[9, 31] additives in electrolytes, and metal oxides.[32-35] Among others, porous carbon can provide ample space for sulfur expansion. It is an effective way of minimizing the loss of active sulfur species. Thus, carbon nanostructures that can host sulfur atoms have been considered the current best approach to generating enhanced electrochemical performance of sulfur cathodes with enhanced long-term cyclic stability. A number of carbon host structures have been studied[36] including reduced graphene oxide, MOF-derived carbon polyhedrons[37], dense graphene sheets[38], polypyrrole/graphene combination[39], and hierarchical free-standing carbon nanotubes[40]. In general, fine tuning the morphologies and structures enable precise anchor of sulfur within these host structures, which provides high electrical conductivity and enough free volume space to allow for the volume changes of the lithiated sulfur. In addition, appropriate heteroatom dopants into carbon facilitate a strong interaction between carbon hosts and LPS likely due to the possible Lewis acid/base relationship between heteroatoms and LPS.[18] Also, abundance of oxygen-rich functional groups on carbon hosts can bind to sulfur in lithium polysulfide.[41] It has been proved that

heteroatom doping, such as nitrogen, in combination with other surface modifications to the carbon materials further mitigate the shuttle effect through donating electrons to adjacent oxygen containing functional groups, and thus favorable for sulfur bonding.[42] It should be noted that metal oxide nanoparticles with reduction potentials above that of lithium polysulfide can encapsulate polysulfides and significantly reduce the capacity fade by minimizing the amount of inactive sulfur species in the electrolyte.[33] Therefore, an effective approach to improving Li-S battery performance is through a combined effort of physical encapsulation and chemical bonding with LPS within multi-heteroatom-doped carbon host structures. Substantial efforts are dedicated to developing a variety of high performance carbon-host S cathodes,[36] however, achieving a long-term cycle stability above a capacity of 1000 mA h g^{-1} at a reasonably high rate still faces a grand challenge.

In this work, we report a novel graphene nanotube (GNT) carbon host for high-performance sulfur cathodes, which is the nitrogen and oxygen co-doped carbon tubes with relatively large diameters (200-500 nm) and further decorated with transition metal species (Fe, Co, or/and Ni). The unique GNT host was found effective to stabilize sulfur and polysulfides within its large tube structures, thereby providing a confined effect to enhance capacity and long-term cyclic stability. Depending on the metal precursors (M: Fe, Co, or/and Ni) used during the synthesis of GNTs, the nanostructures and morphologies of these M-GNTs can be tailored for optimal electrochemical properties in S cathodes. While Ni and Co have been shown to enhance Li-S battery cycle lifetime and rate capability by preventing LPS migration, an addition of Fe into the M-GNTs further enhances battery performance, making multiple metal incorporations as a new avenue to further increase reaction kinetics. Utilizing the FeCoNi-GNTs as a carbon host with a high sulfur loading (up to ~4.5 mg S cm^{-2}) achieved very encouraging Li-S battery performance, showing exceptional

discharge capacities of 1234.7 mAh g^{-1} (5.52 mAh cm^{-2}) at C/20 and 909.0 mAh g^{-1} (4.07 mAh cm^{-2}) at C/5. Also, the FeCoNi-GNTs S cathode exhibited high-rate performance at 2C and enabled exceptional capacity retention at 1C with a discharging capacity of 554.4 mAh g^{-1} after 500 cycles, corresponding to a slow capacity loss at 0.08% per cycle. Large sized and heteroatom doped GNT hosts demonstrated a new strategy to design effective carbon host for high performance Li-S battery cathodes.

2. Experimental details

2.1 Synthesis and characterization of M-GNT carbon hosts

The synthesis of the M-GNTs is detailed in our previous work in an effort to develop carbon-based catalysts for oxygen electrocatalysis.[43-45] Typically we initiate by mixing of metal acetate precursors (anhydrous iron acetate, cobalt acetate tetrahydrate and/or nickel acetate tetrahydrate) at an optimal stoichiometric ratio until reagents are fully dissolved in an aqueous solution. Then dicyandiamide (DCDA), as both carbon and nitrogen sources, is added in the above solution with the temperature set at 60 °C for 4 h, followed by gradual evaporation of water from the solution overnight at 70 °C. The dried mixture was carefully ground in a mortar and pestle, and then heat treated at 1000 °C for 1 h under N_2 flowing gas. Finally, the resulting products were subject to a thorough acidic leaching treatment with 1.0 M HCl at 60 °C for 4 h to remove metallic aggregates and other unstable compounds. After washing with Milli-Q water until ~ pH 7 and drying under vacuum overnight, the samples were stored under Ar before their use for fabricating the S cathode. The samples were labelled as M-GNTs (M: Co, CoNi, and FeCoNi) depending on the types of metals used during the synthesis.

Scanning electron microscopy (SEM) and transmission electron microscopy (TEM) imaging were performed using a Hitachi SU 70 and a JEOL 2100F, respectively, to study morphologies

and nanostructures of these M-GNT with and without hosting S. To further determine elemental distribution in the samples, scanning TEM imaging coupled with energy dispersive X-ray spectroscopy (EDX) elemental mapping were performed with a Thermo Fisher Scientific Talos F200X. Brunauer-Emmett-Teller (BET) surface area and pore size distribution were calculated from the nitrogen absorption and desorption on a Micromeritics TriStar II instrument at 77 K. The samples were degassed at 150 °C for 4 h under vacuum before the BET measurements were taken. Thermo-gravimetric analysis (TGA) (TA Instruments DST Q600 with a ramping rate of 20 °C min^{-1} under N_2 flow) was utilized to determine the sulfur content after infiltration in the carbon host. For TGA analysis, weight loss within the utilized temperature range is attributed to elemental sulfur within the carbon host. X-ray diffraction (XRD) patterns were obtained with a Rigaku Ultima IV diffractometer which uses Cu Kα X-rays (λ = 0.15406 nm) operated at 44 mA and 40 kV. The 2θ range of the XRD measurements was from 10 to 80°. Raman spectroscopy was performed with a Renishaw Raman system with a 514 nm laser source to study carbon structures. X-ray photoelectron spectroscopy (XPS) was performed using a Kratos AXIS Ultra DLD XPS system equipped with a hemispherical energy analyzer and a monochromatic Al Kα source to determine heteroatom dopants and other surfaces species on M-GNTs. The source was operated at 15 keV and 150 W; pass energy was fixed at 40 eV for the high-resolution scans.

2.2 Preparation of sulfur cathodes (S@M-GNTs)

Sulfur infused heteroatom doped graphene nanotubes *i.e.*, S@M-GNTs were prepared by a melting diffusion technique. Sulfur and M-GNTs were mixed in a mortar and pestle (6:4 mass ratio) for 10 to 15 min under Ar atmosphere and then heated to 155 °C for 12 h in an autoclave reactor according to a documented procedure.[22, 28] As a control, sulfur was also infused into a commercial multi-walled carbon nanotube (MWNT) to prepare an S@MWCNTs cathode by using identical

procedures. The MWCNTs were purchased from CheapTubes Inc. (USA) with typical diameter from 8 to 15 nm without heteroatom dopants and transition metal species incorporation.

2.3 Li-S battery cell fabrication and tests

Cathode slurries were prepared by mixing the S@M-GNTs with conductive carbon (Super-P) and polyvinylidene fluoride (PVDF) in N-methyl-2-pyrrolidone (NMP) at a mass ratio of 8:1:1. At first, the dry powders (S@M-GNTs and Super-P) were ground together with a mortar and pestle. The PVDF solution was added then mixed in a FlackTeK Speed Mixer. Then NMP was added and remixed until a spreadable consistency was achieved. The slurries were coated on Al foil and dried at 90°C for one hour in air, then 70 °C overnight under reduced pressure. Three S loadings were prepared in the composite cathodes including ~1.0, 2.0-2.5, and 4.0-5.0 mg S cm^{-2} for Li-S battery studies. CR2032 coin cells for battery studies were assembled in an Ar filled glovebox (<5.0 ppm O_2). A piece of Li metal was used as the anode. The assembled cells utilized a typical Li-S battery electrolyte consisting of 1.0 M LiTFSI in 1,3-dioxolane (DOL)/ Dimethoxy ethane (DME) (vol. = 1:1) with a 2 wt% $LiNO_3$ additive.[46] 50 μL electrolytes were used for the low-sulfur loading cells (*i.e.*, ~30 μL mg S^{-1}), and 200 μL electrolyte were used for the high (~45 μL mg S^{-1}) and ultra-high sulfur loading cells (~25 μL mg S^{-1}). It should be noted that the electrolyte amount used in this work is higher than the most desirable value (10 μL/cm^2) for high gravimetric energy density.[47] Further optimization is ongoing to reduce electrolyte amount while still maintaining performance.

Galvanostatic charge and discharge tests were performed with an Arbin MSTAT battery station at room temperature. The voltage ranges for testing was from 1.7 to 2.7 V for ≥ C/2 and 1.5 – 2.7 V for < C/2. Each cell was preconditioned at C/20 for one cycle before cycle lifetime testing. Cyclic voltammetry (CV) was performed in the range of 1.5–3.0 V on a CHI electrochemical

station with a scan rate of 0.5 mV s^{-1}. Electrochemical impedance spectroscopy (EIS) was performed on a Metrohm Autolab NOVA from 1.0 Hz to 100 kHz at room temperature.

3. Results and Discussion

3.1 Structure and morphology of M-GNT carbon hosts

A schematic of the preparation of the S@M-GNT material is displayed in **Figure 1**. Briefly, the nitrogen-doped and large-sized GNTs were prepared via a carbonization of dicyandiamide (DCDA- a dimer of cyanamide) at 1000 °C for 1 h under flowing N_2 environments.[43] During the synthesis, various metals acetates (Fe, Co or/and Ni) were used as the source of transition metal that catalyze the formation of GNTs. Among the studied metal combinations for the synthesis of GNTs, Co, CoNi, and FeCoNi based GNTs were highlighted in this work to compare their characteristics as an ideal carbon host for sulfur cathodes in Li-S batteries. Then, sulfur infiltration was carried out to fill sulfur into these tubes.

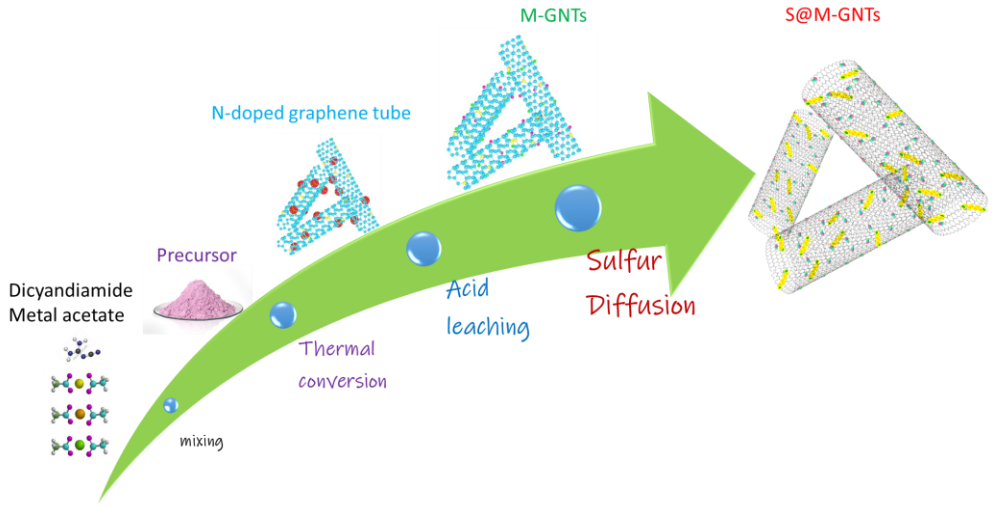

Figure 1. A synthetic scheme of S@M-GNT cathode for Li-S batteries.

Morphologies and microstructures of the as prepared M-GNTs and S-containing M-GNTs were characterized first by using HR-TEM and SEM images (**Figure 2,** S1, and S2). The diameter and

wall thickness of GNTs are largely dependent on the use of metals during the synthesis according to the close observation of the layered graphitic structures by using HR-TEM images (**Figure S3**). Compared to single Co and binary CoNi, the ternary FeCoNi alloys result in the thickest walls of tubes potentially beneficial for corrosion resistance enhancement and favorable surface dopants. Also, the ternary FeCoNi-GNTs show the largest tube diameters approximately 200-500 nm, ideally for stabilizing S and LPS within cathodes. Although acidic leaching treatments were taken, metal/alloy nanoparticles are still apparent and enclosed into the M-GNTs based on the high resolution HR-TEM images (**Figure S4**) and STEM-EDX elemental maps (**Figure S5, S6,** and **S7**). After the sulfur infiltration process, part of tubes is filled with S, which is confined inside of the tubes according to the TEM images shown in **Figure 2d** to **2f**.

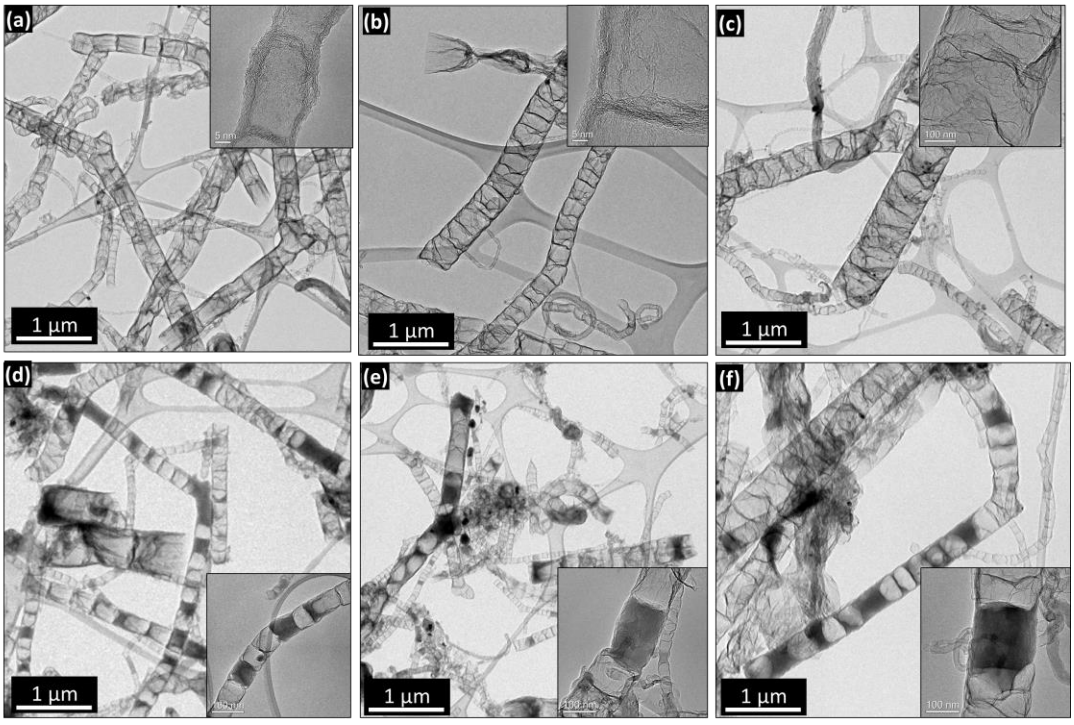

Figure 2. TEM images for various large-sized graphene tubes (a-c) before and (d-f) after accomodating S as cathodes for Li-S batterties. (a) Co-GNTs, (b) CoNi-GNTs, (c) FeCoNi-GNTs,

(d) S@Co-GNTs, (e) S@CoNi-GNTs, and (f) S@FeCoNi-GNTs. The corresponding inserts show more detailed structures of the graphene tubes with and without hosting S.

The best performing FeCoNi-GNTs were studied by using by using STEM images and corresponding elemental mapping as shown in **Figure 3**. The doped N and O along with decoration of metallic particles are apparent on the FeCoNi-GNTs. The presence of nitrogen and oxygen in the bulk carbon structure is due to the possible doping during the carbonization process of DCDA.[43] Also, FeCoNi alloy particles are throughout the bulk tubes, and they have an average diameter of approximately 10-30 nm (Figure 3 and **Figure S7**). Oxygen was found enriched on the particles showing the possible oxide films onto metallic alloy particles. In addition to the crystalline FeCoNi alloys particles, atomically dispersed Fe, Co, and Ni sites are likely well dispersed into the GNTs (**Figure S8**), which are coordinated with nitrogen in the form of MN_x sites similar to the active sites in well-studied M-N-C catalysts.[48-50] After incorporating S into FeCoNi-GNTs, their STEM images along with EDX mapping are shown in **Figure 4** and **Figure S9** at different parts of GNT samples, further verifying that the carbon host is able to encapsulate the sufficient amount of sulfur active material. The elemental qualification of the S@FeCoNi-GNT is listed in Table S1. The nitrogen and oxygen contents are 4.7 and 3.0 wt%, respectively. The total content of metals is around 1.6 wt%. The others are carbon and sulfur. Similar morphologies of S encapsulation in tubes were observed with the S@Co-GNT (**Figure S10**) and S@CoNi-GNT samples (**Figure S11**). Compared to other studied carbon hosts, encasing of sulfur within a tube structure is a beneficial property for M-GNTs, as it can lead to the physical encapsulation of LPS during the reversible battery reactions, which enhance cyclic stability of Li-S batteries.[31]

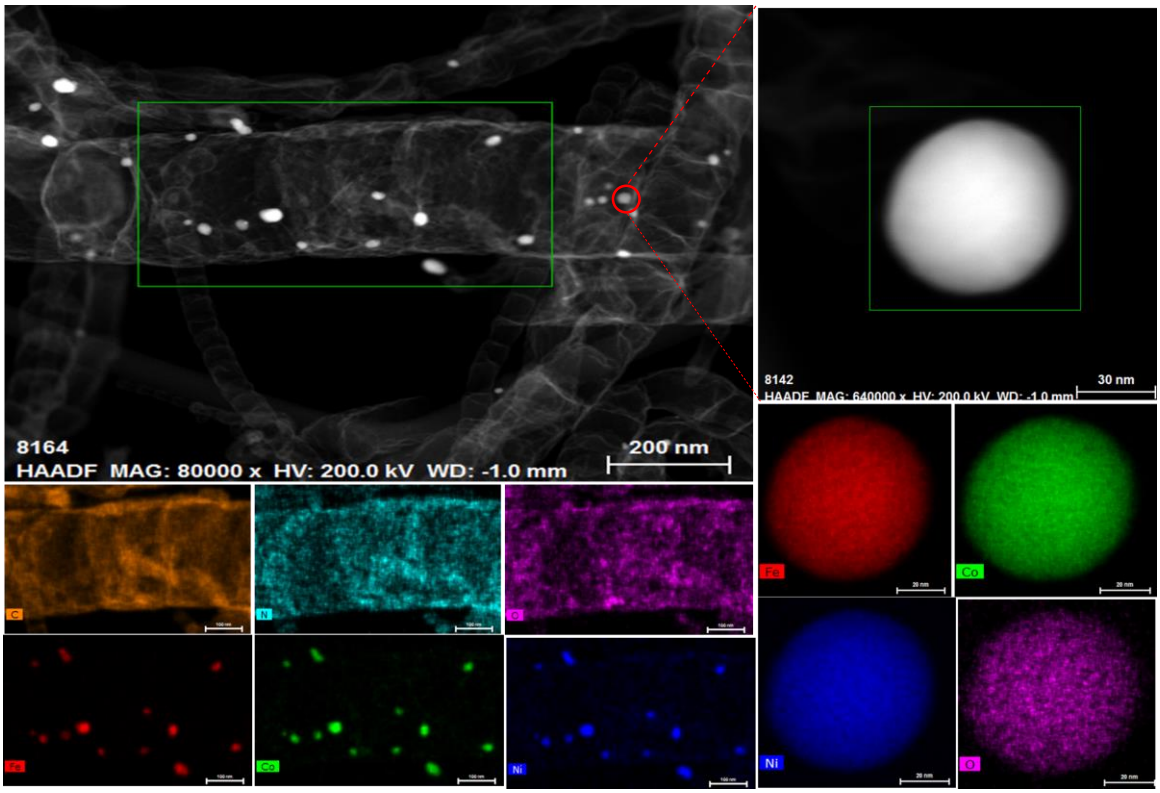

Figure 3. STEM-EDX mapping for the as prepared FeCoNi-GNTs showing best performance being a host for S cathode. The brightly colored metal nanoparticles on the surface of the FeCoNi-GNTs material are composed of FeCoNi alloys identified through showing Fe (red), Co (green), and Ni (blue) atoms.

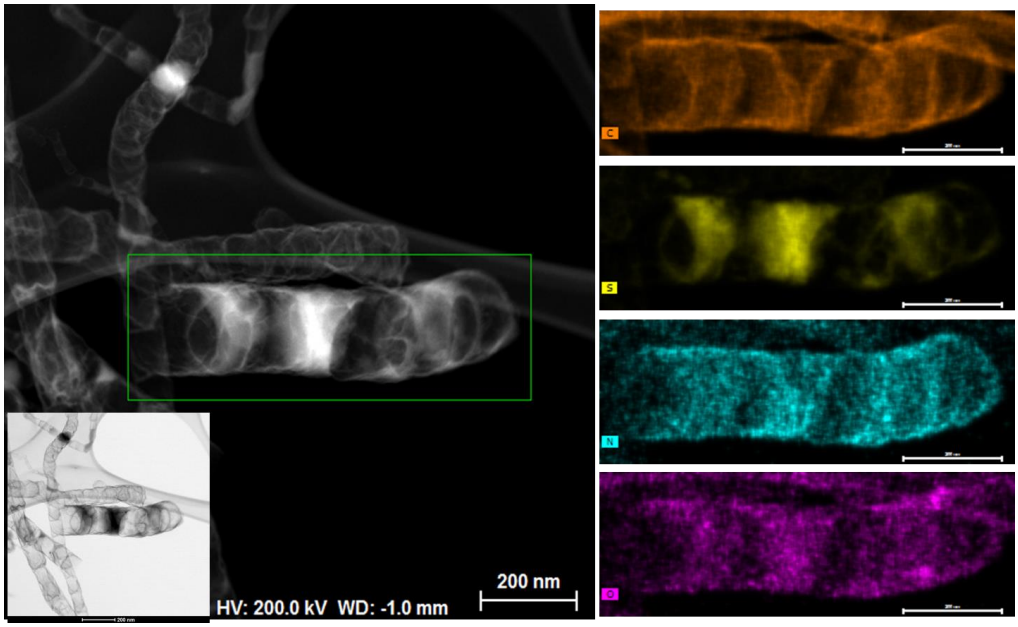

Figure 4. STEM-EDX mapping for S@FeCoNi-GNTs containing S inside the tubes. The carbon (orange) tube-structure is visible with N (turquoise) and O (pink) doping present throughout. Sulfur (yellow) has diffused, via melting, into the tube-structure which allows for excellent contact with the carbon hosts structure.

XRD analysis was performed on all M-GNT samples, and their typical results are shown in **Figure 5 (a)**. The 26.5° peak for each case is the (002) plane of graphitic carbon. Peaks at 44.4°, 51.7°, and 76.2° for Co-GNTs can be indexed to the (111), (200), and (220) planes respectively, of metallic Co.[17] Peaks at 44.7°, 51.9°, and 76.4° for CoNi-GNTs can be indexed to the (111), (200), and (220) planes respectively, of metallic CoNi alloy.[43] Likewise, peaks at 44.1°, 51.5°, and 75.6° for FeCoNi-GNTs match closely with reported peaks for ternary FeCoNi alloys.[43] The slight shifts of peaks among three M-GNTs are due to the formation of FeCoNi and CoNi alloys when compared to single Co metals. Raman spectra were performed on each M-GNTs material and shown in **Figure 5b**. All GNTs show dominant D-band (~1350 cm^{-1}), G-band (~1580 cm^{-1}), and

G′-band (~2700 cm^{-1}) peaks. The G-band represents graphitic carbon, while the D-band represents induced disorder in the structure, typically due to edge sites and defects of carbon planes as well as the heteroatom dopants.[51] FeCoNi-GNTs shows the highest D/G band ratio, indicating the highest degree of doping, which is in good agreement with XRD analysis. In addition, the G′/G ratio can be used to determine the thickness of the walls of the carbon structure where a lower ratio correlates to a higher number of walls.[52] Compared to other M-GNTs, the FeCoNi-GNT exhibits the smallest G′/G ratio and, therefore, the thickest, or highest number, of walls which is in agreement with the HR-TEM images (Figure S3).

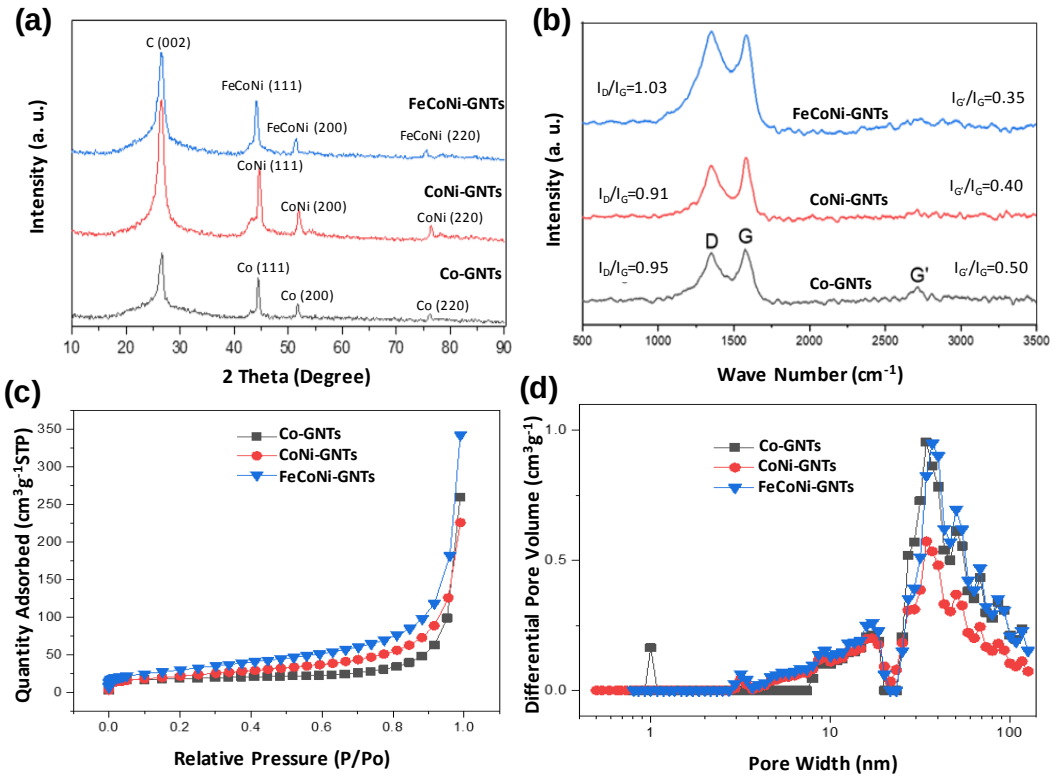

Figure 5. Structures and morphologies of the studied Co-GNTs, CoNi-GNTs, and FeCoNi-GNT samples. (a) XRD patterns, (b) Raman spectra, (c) BET surface areas, and (d) pore volume and distribution.

The BET surface areas (**Figure 5c**) and pore volumes (**Figure 5d)** for the studied M-GNT samples are analyzed. The FeCoNi-GNT carbon exhibit the largest surface area (108 m^2 g^{-1}) and pore volume (0.437 cm^3 g^{-1}), when compared to CoNi-GNTs (78 m^2 g^{-1} and 0.282 cm^3 g^{-1}) and Co-GNTs (63 m^2 g^{-1} and 0.395 cm^3 g^{-1}). N_2 absorption and desorption isotherms for each M-GNT and MWNT material are compared in **Figure S12**. The high surface area and the large pore volume of the FeCoNi-GNT material can theoretically expose increased number of sites to anchor LPS than the Co-GNTs and CoNi-GNTs. It can also provide significantly increased surface areas for the precipitation reaction product, Li_2S_2, to nucleate and grow on the carbon host. In addition, the FeCoNi-GNT host can accommodate the largest amount of S within the pores of the material due to its high pore volume and dominant mesopores, leading to a high utilization of the sulfur active material. It appears, therefore, logically that the large pore volume, large tube diameter, and high surface area of the FeCoNi-GNT carbon host makes it the optimal material for high-performance Li-S batteries. This is verified through electrochemical testing as discussed below.

XPS C1s and N1s analyses were performed on the studied M-GNT samples and shown in **Figure 6**. For each M-GNT, C1s spectra can be deconvoluted with C=C (284.6 eV), C-C (285.5 eV), C-N (285.5 eV), C-O (286.7 eV), O-C=O (288.3 eV), carbonates (290.0 eV), and π-π* transitions (291.8 eV) peaks, reflecting the diverse structures of carbon in the M-GNTs. The π-π* transitions indicate the interactions between the graphene layers which comprise the M-GNTs tube structure.[43] In good agreement with XRD and Raman results , all of the M-GNTs present similar graphitized C=C strucures along with identifiable C-N and C-O species. As for N1s spectra, pyridinic (~398.7 eV) and graphitic (~401.2 eV) N are dominant, indicating the major dopants of

nitrogen are located at the edge and interior of carbon planes, respectively. In addiiton, oxidized pyridinic nitrogen (~405.5 eV) can be detected. These three types of doped nitrogen species in the M-GNTs may associaed with the enhanced LPS adsorption to the carbon host surface. Generally, N-doping allows the chemadsorption of the LPS on the surface of the carbon host material where it can be further oxidized or reduced at the cathode.[18] The LPS is chemabsorbed due to a Lewis acid/base relationship between the N-dopants and the LPS. The percent ratios of each nitrogen species are reported in **Table S2**. Compared to the others, FeCoNi-GNTs present more dominant graphtic N dopants due to the addition of Fe species in good agreement with our previous observation.[53] It was reported that, compared to pyridinic N, the graphitic N sites in the carbon hosts have stronger capability to bind LPS,[54] which is in line with the improved battery performance measured with the FeCoNi-GNT hosts. In a similar manner to N-dopants, O-dopants also can retain LPS at the cathode during cycling.[55] TGA analyses were carried out for the S@FeCoNi-GNT cathode to determine the weight percentage of sulfur in the M-GNTs material after melt diffusion (**Figure S13**). The S@FeCoNi-GNTs material was typically composed of ~56 wt% S, which is close to 60 wt.% initially mixed with the carbon host.

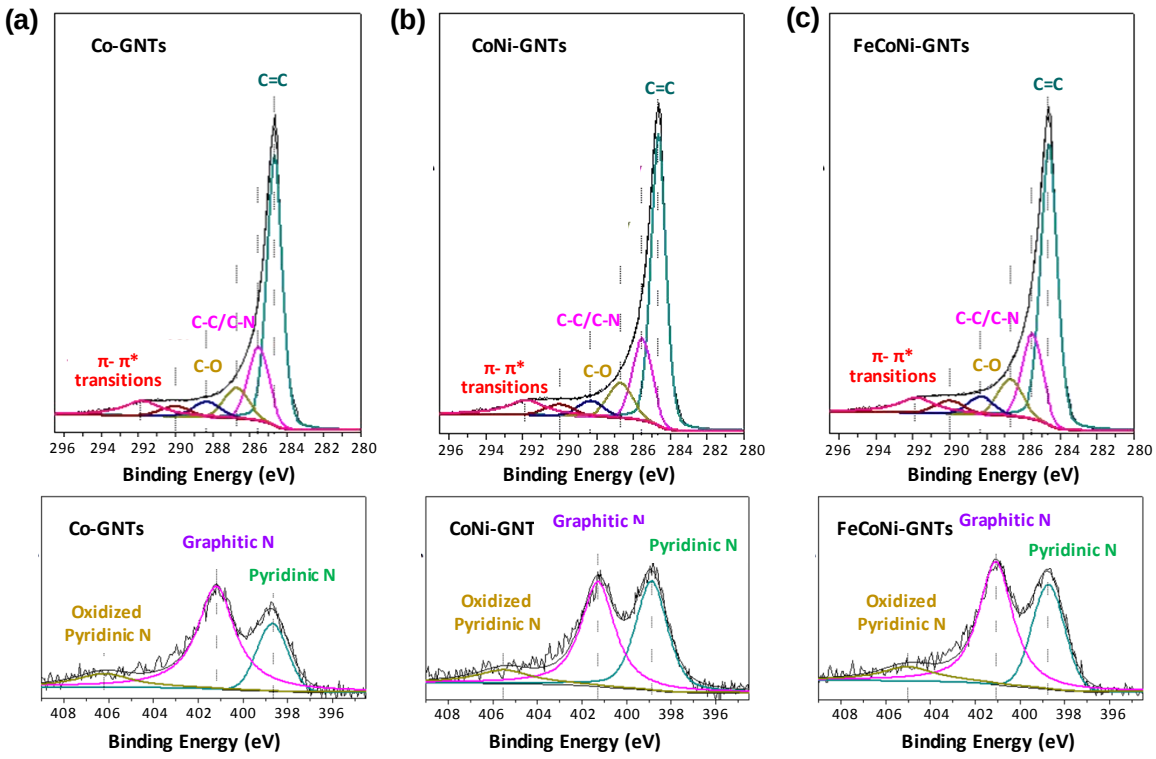

Figure 6. The C1s and N1s XPS spectra of Co-GNTs (a), CoNi-GNTs (b), and FeCoNi-GNTs (c).

3.2 Electrochemical Performance

The electrochemical performance of the S@M-GNTs cathodes was studied versus a lithium metal anode in Li-S coin cells. Rate capability (1C = 1670 mA g^{-1}) was carried out at C/20, C/5, C/2, 1C, and 2C. A comparison of S@Co-GNTs, S@CoNi-GNTs, S@FeCoNi-GNTs, and S@MWCNTs is presented in **Figure 7a**. The discharge capacity of S@MWCNTs cathode drops drastically when increasing the rate from C/5 to C/2, likely due to weaker interactions of LPS with carbon hosts upon cycling and less favorable smaller tube sizes (8-15 nm) of the commercial MWNTs. All S@M-GNTs cathodes display the ability to operate at high C-rates (up to 2C) as the two plateau regions can be clearly seen in each discharge cycle **(Figure S14)**. It should be noted that we have systematically investigated the effect of metals on battery performance including individual Co,

Ni, and Fe-GNT as shown in **Figure S15**. Compared to binary and ternary metals-based GNTs, the individual metal-derived GNTs exhibited inferior capacity and less stable cyclic performance. The possible reasons are likely the smaller tube diameter sizes and undesirable metal and heteroatom doping. Among the studied samples, the FeCoNi-GNT material allows for the highest initial discharge capacity of 668.9 mAh g^{-1} at 2C.

Long term galvanostatic charge and discharge cyclic stability was first studied at a C/5 rate with a low sulfur loading (~1.0 mg S cm^{-2}). Initially discharge capabilities for each sample are 1014.2 mAh g^{-1} for S@MWCNTs, 1048.8 mAh g^{-1} for FeCoNi-GNTs, 971.6 mAh g^{-1} for CoNi-GNTs, and 917.0 mAh g^{-1} for Co-GNTs (**Figure 7b**). After 50 cycles, the discharge capacities were reduced to 755.0 mAh g^{-1} for S@MWCNTs, 964.8 mAh g^{-1} for FeCoNi-GNTs, 875.2 mAh g^{-1} for CoNi-GNTs, and 760.1 mAh g^{-1} for Co-GNTs. The capacity retention of FeCoNi-GNTs is the highest, up to 92.0% after 50 cycles, when compared to MWCNT and other M-GNT hosts. The 1^{st}, 5^{th}, 25^{th}, and 50^{th} discharge voltage profiles of the S@FeCoNi-GNT cathode (**Figure S16**) show that there is little change in the discharge capacity and voltage profiles over 50 discharge cycles at a reasonable rate of C/5. The superior reversibility is achieved by the combined effects including N- and O-doping and presence of transition metal (FeCoNi) species in the GNT host. As discussed above, such heteroatom doping including N and O are uniformly dispersed onto the GNTs, which are able to increase the performance of cathodes primarily because of its ability to bind to LPS products during cycling. Heteroatom doping also has a secondary role in facilitating electron transfer kinetics, allowing for enhanced electron conductivity through the cathode, which also prevents structural degradation of the cathode over time. There are two types of metal species in the GNTs including metallic nanoparticles enclosed into the tubes and atomically dispersed atomic metal MN_4 sites stabilized by nitrogen dopants. Apart from metallic and metal oxides

capable of strengthening the interaction of LPS with carbon hosts,[32, 33, 56] the uniform dispersed MM_4 sites may be more important to facilitate adsorption of S and LPS due to their well-known capability to adsorb O_2 and CO_2 molecules containing electron-negative elements. It could also facilitate the electrocatalysis process to convert the LPS to insoluble Li_2S_2 and Li_2S within cathodes.[49]

Furthermore, high loadings (2.0-2.5 mg S cm^{-2}) of S@FeCoNi-GNTs and S@MWCNTs were utilized to determine the effect of increased sulfur loading on performance, and they were tested at a rate of C/5 (**Figure 7c**). The high loading S@FeCoNi-GNT cathode displayed 90.7% capacity (882.3 mAh g^{-1}) measured at the low loading S@FeCoNi-GNT cathode (~mg S cm^{-2}) after the 50th cycle. This demonstrated the excellent capability of FeCoNi-GNT hosts for high S loading without compromise of electrochemical performance, which often is a grand challenge for other types of carbon hosts. In an attempt to maximize areal capacity (mAh cm^{-2}), ultra-high S loading at ~4.5 mgS cm^{-2} for FeCoNi-GNTs were prepared and tested for long-term cycle lifetime. The ultra-high sulfur loading S@FeCoNi-GNT cathode discharged 1234.7 mAh g^{-1} (5.52 mAh cm^{-2}) at C/20 and 909.0 mAh g^{-1} (4.07 mAh cm^{-2}) at C/5 (**Figure S17**). Especially, after ten cycles at C/5, a capacity of 828.0 mAh g^{-1} (3.70 mAh cm^{-2}) was retained, which is higher than reported values in the literature for ultra-high sulfur loading Li-S cells.[57] Also, there is a negligible difference at C/5 when increasing the S loadings from high to ultra-high after 10 cycles. Due to the high areal capacity achieved, the S@FeCoNi-GNTs cathode could be useful in practical applications.

CV curves was measured for the S@FeCoNi-GNT cathode at a scanning rate of 0.5 mV s^{-1} for first five cycles (**Figure 7d**). The anodic peak at ~2.65 V is attributed to the oxidation of Li_2S to S_8. The two cathodic peaks are attributed to the reduction of S_8 to LPS (~2.25 V), and the further reduction of LPS to Li_2S_2 and Li_2S (~1.85 V). The peak positions and current profiles during the

five cycles are nearly overlapped, thus further verifying the excellent electrochemical reversibility of sulfur cathodes within the M-GNT carbon host. In addition, the gradually increased peak intensity during the cycling indicates the enhanced kinetics of the oxidation and reductions of the active material. This is a further proof that the FeCoNi-GNT carbon host greatly improves the kinetics of the precipitation reaction. In addition, EIS (**Figure S18**) of full Li-S cells shows that the S@FeCoNi-GNT cathode has the lowest resistivity after rate capability testing when compared to CoNi-GNTs and Co-GNTs.

Finally, long term cycle lifetime tests at a rate of 1C was performed on all S@M-GNT cathodes and are compared in **Figure 8g**. S@MWCNTs was not tested as it polarized quickly at rates larger than C/2. The 1C initial discharge capacities were 955.5 mAh g^{-1} for S@FeCoNi-GNTs, 748.5 mAh g^{-1} for S@CoNi-GNTs, and 726.7 mAh g^{-1} for Co-GNTs. After 500 cycles the discharge capacities were retained at 554.4 mAh g^{-1} for FeCoNi-GNTs, 362.9 mAh g^{-1} for CoNi-GNTs, and 452.2 mAh g^{-1} for Co-GNTs. Once again, the S@FeCoNi-GNT cathode displays extraordinary discharge capacity retention at 1 C with a slow degradation rate of 0.08 % capacity loss per cycle. The encouraging long-term cyclic stability and capacity at a relatively high rate of 1C is attributed to many unique properties discussed above for the FeCoNi-GNT host including the largest geometric diameter in tubes, the highest surface areas and pore volumes, dominant mesopores, appropriate N and O doping especially the favorable graphitic N, FeCoNi alloy particles enclosed in the tubes, and the likely atomically dispersed MN_4 active sites. The overall battery performance metrics of S@FeCoNi-GNT cathodes were further compared to those of reported for heteroatom-doped and metal nanoparticle decorated carbon hosts at 1C (**Table S3**), representing one of the best performing carbon hosts for Li-S batteries.

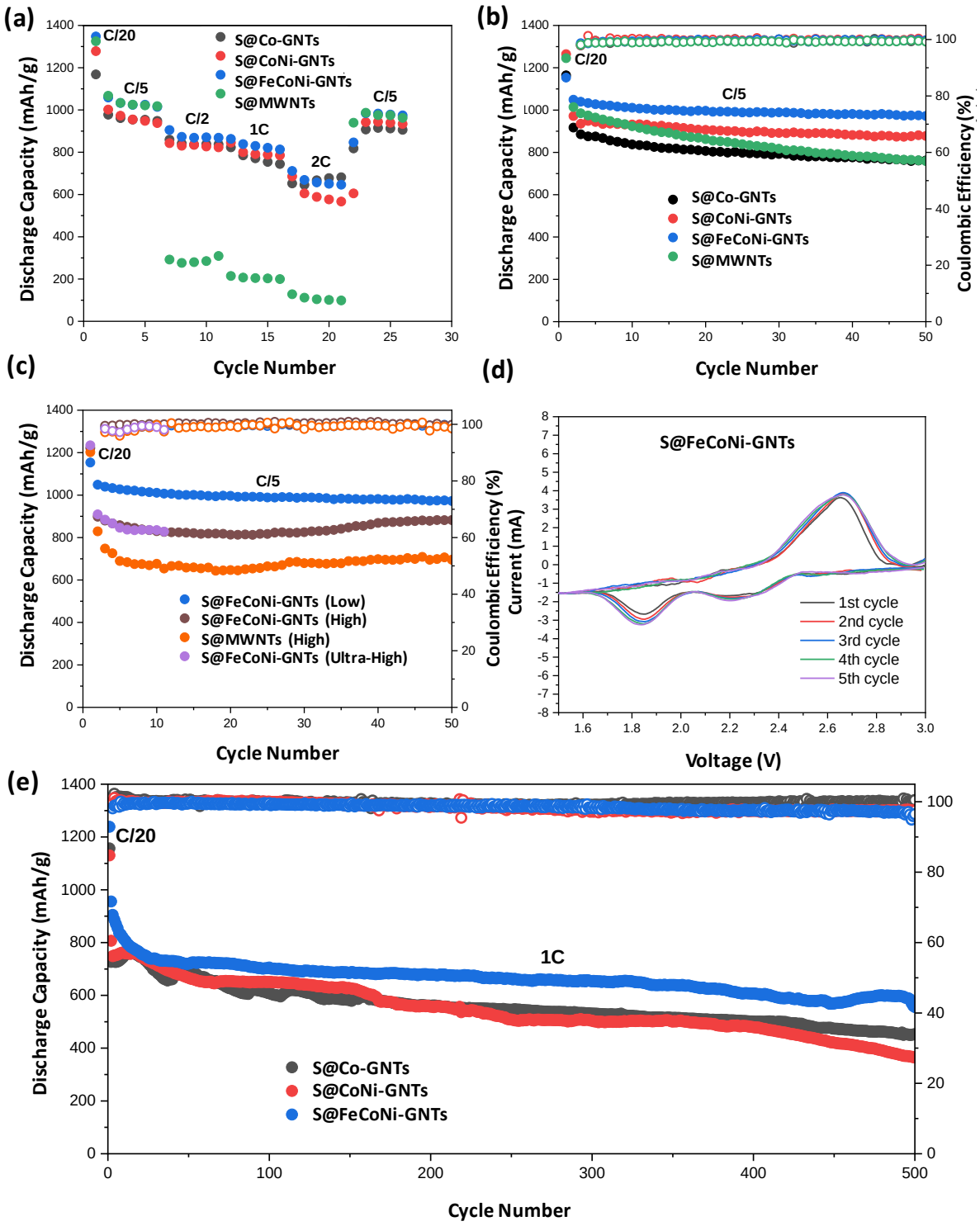

Figure 7. (a) Rate capability of S@Co-GNTs, S@CoNi-GNTs, S@FeCoNi-GNTs, and S@MWCNTs at C/20, C/5, C/2, 1C, and 2C. (b) Cycle lifetime testing and Coulombic efficiency of low sulfur loading S@Co-GNTs, S@CoNi-GNTs, S@FeCoNi-GNTs, and S@MWCNTs at C/5

(~1.0 mg S cm^{-2}). (c) Cycle lifetime and Coulombic efficiency of high loading S@MWCNTs and low (~1.0 mg S cm^{-2}), high (2.5-2.7 mg S cm^{-2}), and ultra-high loadings (~4.5 mgS cm^{-2}) of S@FCN-GNTs at C/20 for the first cycle and then at C/5. (d) Cyclic voltammetry of S@FeCoNi-GNTs from 1.5 to 3.0 V for five cycles with a scan rate of 0.5 mV s^{-1}. (e) Cycle lifetime and Coulombic efficiency of ultra-high sulfur loading S@Co-GNTs, S@CoNi-GNTs, and S@FeCoNi-GNTs at 1C.

4. Conclusions

In summary, this work reports a new type of effective nanocarbon host for sulfur cathodes to address the insufficient capacity and cyclic stability issues of current Li-S batteries especially at a practically high sulfur loading. The heteroatom (*e.g.*, N and O) doped graphene tubes with relatively larger diameters (200-500 nm) decorated with FeCoNi nanoparticles and atomically dispersed metal sites likely in the form of MN_4 were studied as effective carbon hosts for S cathode showing encouraging rate performance and cyclic stability in Li-S batteries. It was found that the diameter of GNTs are greatly dependent on the metal sources used for the synthesis of GNTs. Compared to Co and CoNi, ternary FeCoNi yields the largest diameters and the thickest wall of tubes. As a result, the unique large tube size along with increased surface areas and pore volumes with dominant mesopores benefit from the facile incorporation of S into the GNT hosts. Thus, the graphene tube can host sufficient amount of S within the tubes yet leaving room for volume expansion of S cathodes during lithiation. The richness of nitrogen doping[54, 58] and surface oxygen functional groups[59] along with the modification of FeCoNi alloys and atomic metal sites [49, 56] can enhance the interaction between the nanocarbon host and sulfur/polysulfides. Therefore, the S@FeCoNi-GNT cathode at an ultra-high S loading (~4.5 mg S cm^{-2}) is able to yield very

encouraging battery performance. The metrics includes the initial discharge-capacities of 1234.7 mAh g^{-1} (5.52 mAh cm^{-2}) at C/20 and 909.0 mAh g^{-1} (4.07 mAh cm^{-2}) at C/5. After 500 cycles at a rate of 1C, the S@FeCoNi-GNT cathode still retains a capacity of 554.4 mAh g^{-1}, corresponding a very slow degradation rate of 0.08% per cycle. Compared to Co and CoNi derived graphene tubes, the addition of Fe likely further improves the capacity retention of S@M-GNT cathodes through providing more favorable graphitic N and active atomic FeN_4 sites, therefore enhancing electrochemical reaction kinetics and chemically/physically encapsulating the sulfur active material. The FeCoNi-derived GNT host newly developed in this work demonstrated exceptional capability to host sulfur at an ultra-high loading with improved cyclic stability at a high-rate, which would shed light on the development of high-performance Li-S batteries.

Acknowledgements

We would like to thank the support from the National Science Foundation (CBET-1604392) along with the Sustainable Manufacturing and Advanced Robotics Technology (SMART) Community of Excellence program at the University at Buffalo, SUNY. Electron microscopy works were conducted at the Center for Functional Nanomaterials, which is a U.S. DOE Office of Science Facility, at Brookhaven National Laboratory under Contract No. DE-SC0012704.

References

1. N. Nitta, F. Wu, J. T. Lee and G. Yushin, *Materials today*, 2015, **18**, 252-264.
2. G. Chen, J. An, Y. Meng, C. Yuan, B. Matthews, F. Dou, L. Shi, Y. Zhou, P. Song, G. Wu and D. Zhang, *Nano Energy*, 2019, **57**, 157-165.
3. Z. Yang, R. Li and Z. Deng, *Scientific reports*, 2018, **8**, 863.
4. D. Aurbach, *Journal of The Electrochemical Society*, 2018, **165**, Y1-Y1.

5. X. Fan, W. Sun, F. Meng, A. Xing and J. Liu, *Green Energy & Environment*, 2018, **3**, 2-19.

6. H. Zhao, N. Deng, J. Yan, W. Kang, J. Ju, Y. Ruan, X. Wang, X. Zhuang, Q. Li and B. Cheng, *Chemical Engineering Journal*, 2018.

7. M. Agostini, D. H. Lim, M. Sadd, J.-Y. Hwang, S. Brutti, J. Heo, J.-H. Ahn, Y.-K. Sun and A. Matic, *ChemSusChem*, 2018.

8. B.-Q. Li, S.-Y. Zhang, L. Kong, H.-J. Peng and Q. Zhang, *Advanced Materials*, 2018, **30**, 1707483.

9. X. L. Ji, K. T. Lee and L. F. Nazar, *Nature Materials*, 2009, **8**, 500-506.

10. N. Jayaprakash, J. Shen, S. S. Moganty, A. Corona and L. A. Archer, *Angewandte Chemie International Edition*, 2011, **50**, 5904-5908.

11. L. Ji, M. Rao, H. Zheng, L. Zhang, Y. Li, W. Duan, J. Guo, E. J. Cairns and Y. Zhang, *Journal of the American Chemical Society*, 2011, **133**, 18522-18525.

12. J. Schuster, G. He, B. Mandlmeier, T. Yim, K. T. Lee, T. Bein and L. F. Nazar, *Angewandte Chemie International Edition*, 2012, **51**, 3591-3595.

13. H. Wang, Y. Yang, Y. Liang, J. T. Robinson, Y. Li, A. Jackson, Y. Cui and H. Dai, *Nano letters*, 2011, **11**, 2644-2647.

14. C. Zhang, H. B. Wu, C. Yuan, Z. Guo and X. W. Lou, *Angewandte Chemie*, 2012, **124**, 9730-9733.

15. Y. Chen, S. Lu, J. Zhou, X. Wu, W. Qin, O. Ogoke and G. Wu, *Journal of Materials Chemistry A*, 2017, **5**, 102-112.

16. L. F. Nazar, M. Cuisinier and Q. Pang, *MRS Bulletin*, 2014, **39**, 436-442.

17. S. Liu, J. Li, X. Yan, Q. Su, Y. Lu, J. Qiu, Z. Wang, X. Lin, J. Huang and R. Liu, *Advanced Materials*, 2018, **30**, 1706895.

18. M. Zhang, C. Yu, C. Zhao, X. Song, X. Han, S. Liu, C. Hao and J. Qiu, *Energy Storage Materials*, 2016, **5**, 223-229.

19. K. Xiang, S. Cai, X. Wang, M. Chen and S. Jiang, *Journal of Alloys and Compounds*, 2018, **740**, 687-964.

20. M.-E. Zhong, J. Guan, Q. Feng, X. Wu, Z. Xiao, W. Zhang, S. Tong, N. Zhou and D. Gong, *Carbon*, 2018, **128**, 86-96.

21. J. H. Zhang, M. Huang, B. J. Xi, K. Mi, A. H. Yuan and S. L. Xiong, *Advanced Energy Materials*, 2018, **8**, 1701330.

22. H. D. Yuan, W. K. Zhang, J. G. Wang, G. M. Zhou, Z. Z. Zhuang, J. M. Luo, H. Huang, Y. P. Gan, C. Liang, Y. Xia, J. Zhang and X. Y. Tao, *Energy Storage Materials*, 2018, **10**, 1-9.

23. R. Yang, L. Li, D. Chen, L. P. Chen, B. Ren, Y. L. Yan and Y. H. Xu, *ChemistrySelect*, 2017, **2**, 11697-11702.

24. M. D. Walle, Z. Zhang, M. Zhang, X. You, Y. Li and Y.-N. Liu, *Journal of Materials Science*, 2018, **53**, 2685-2696.

25. R.-S. Song, B. Wang, T.-T. Ruan, L. Wang, H. Luo, F. Wang, T.-T. Gao and D.-L. Wang, *Applied Surface Science*, 2018, **427**, 396-404.

26. M. Xiang, Y. Wang, J. Wu, Y. Guo, H. Wu, Y. Zhang and H. Liu, *Electrochimica Acta*, 2017, **227**, 7-16.

27. U. Gulzar, T. Li, X. Bai, M. Colombo, A. Ansaldo, S. Marras, M. Prato, S. Goriparti, C. Capiglia and R. Proietti Zaccaria, *ACS Applied Materials & Interfaces*, 2018, **10**, 5551-5559.

28. M. Feng, H. J. Li, M. Huang, J. W. Kang, H. G. Feng, Q. M. Su, F. M. Zhang and G. H. Du, *Materials Research Bulletin*, 2018, **99**, 429-435.

29. X. N. Tang, Z. H. Sun, S. P. Zhuo and F. Li, *New Carbon Materials*, 2017, **32**, 535-541.

30. Y. Zhong, X. Xia, S. Deng, J. Zhan, R. Fang, Y. Xia, X. Wang, Q. Zhang and J. Tu, *Advanced Energy Materials*, 2018, **8**, 1701110.

31. J. Zheng, M. Gu, M. J. Wagner, K. A. Hays, X. Li, P. Zuo, C. Wang, J.-G. Zhang, J. Liu and J. Xiao, *Journal of The Electrochemical Society*, 2013, **160**, A1624-A1628.

32. F. Ma, J. S. Liang, T. Y. Wang, X. Chen, Y. N. Fan, B. Hultman, H. Xie, J. T. Han, G. Wu and Q. Li, *Nanoscale*, 2018, **10**, 5634-5641.

33. X. Liang and L. F. Nazar, *ACS Nano*, 2016, **10**, 4192-4198.

34. K. Sun, Q. Zhang, D. C. Bock, X. Tong, D. Su, A. C. Marschilok, K. J. Takeuchi, E. S. Takeuchi and H. Gan, *Journal of The Electrochemical Society*, 2017, **164**, A1291-A1297.

35. K. Sun, M. Fu, Z. Xie, D. Su, H. Zhong, J. Bai, E. Dooryhee and H. Gan, *Electrochimica Acta*, 2018, **292**, 779-788.

36. O. Ogoke, G. Wu, X. L. Wang, A. Casimir, L. Ma, T. P. Wu and J. Lu, *Journal of Materials Chemistry A*, 2017, **5**, 448-469.

37. Z. Li, C. Li, X. Ge, J. Ma, Z. Zhang, Q. Li, C. Wang and L. Yin, *Nano Energy*, 2016, **23**, 15-26.

38. H. Li, X. Yang, X. Wang, M. Liu, F. Ye, J. Wang, Y. Qiu, W. Li and Y. Zhang, *Nano Energy*, 2015, **12**, 468-475.

39. Y. Zhang, Y. Zhao, A. Konarov, D. Gosselink, H. G. Soboleski and P. Chen, *Journal of Power Sources*, 2013, **241**, 517-521.

40. Z. Yuan, H. J. Peng, J. Q. Huang, X. Y. Liu, D. W. Wang, X. B. Cheng and Q. Zhang, *Advanced Functional Materials*, 2014, **24**, 6105-6112.

41. G. Zhou, S. Pei, L. Li, D.-W. Wang, S. Wang, K. Huang, L.-C. Yin, F. Li and H.-M. Cheng, *Advanced Materials*, 2014, **26**, 625-631.

42. S. N. Talapaneni, T. H. Hwang, S. H. Je, O. Buyukcakir, J. W. Choi and A. Coskun, *Angewandte Chemie International Edition*, 2016, **55**, 3106-3111.

43. S. Gupta, L. Qiao, S. Zhao, H. Xu, Y. Lin, S. V. Devaguptapu, X. Wang, M. T. Swihart and G. Wu, *Advanced Energy Materials*, 2016, **6**, 1601198.

44. S. Gupta, S. Zhao, X. X. Wang, S. Hwang, S. Karakalos, S. V. Devaguptapu, S. Mukherjee, D. Su, H. Xu and G. Wu, *ACS Catalysis*, 2017, **7**, 8386-8393.

45. X. Wang, Q. Li, H. Pan, Y. Lin, Y. Ke, H. Sheng, M. T. Swihart and G. Wu, *Nanoscale*, 2015, **7**, 20290-20298.

46. D.-W. Wang, Q. Zeng, G. Zhou, L. Yin, F. Li, H.-M. Cheng, I. R. Gentle and G. Q. M. Lu, *Journal of Materials Chemistry A*, 2013, **1**, 9382-9394.

47. M. Agostini, J.-Y. Hwang, H. M. Kim, P. Bruni, S. Brutti, F. Croce, A. Matic and Y.-K. Sun, *Advanced Energy Materials*, 2018, **8**, 1801560.

48. Y. He, S. Hwang, D. A. Cullen, M. A. Uddin, L. Langhorst, B. Li, S. Karakalos, A. J. Kropf, E. C. Wegener, J. Sokolowski, M. Chen, D. Myers, D. Su, K. L. More, G. Wang, S. Litster and G. Wu, *Energy & Environmental Science*, 2019, **12**, 250-260.

49. Z. Liu, L. Zhou, Q. Ge, R. Chen, M. Ni, W. Utetiwabo, X. Zhang and W. Yang, *ACS Applied Materials & Interfaces*, 2018, **10**, 19311-19317.

50. H. Zhang, S. Hwang, M. Wang, Z. Feng, S. Karakalos, L. Luo, Z. Qiao, X. Xie, C. Wang, D. Su, Y. Shao and G. Wu, *Journal of the American Chemical Society*, 2017, **139**, 14143-14149.

51. A. Ariharan, B. Viswanathan and V. Nandhakumar, *Graphene*, 2017, **6**, 41.

52. M. Chen, S. Hwang, J. Li, S. Karakalos, K. Chen, Y. He, S. Mukherjee, D. Su and G. Wu, *Nanoscale*, 2018, **10**, 17318-17326.

53. G. Wu, M. Nelson, S. Ma, H. Meng, G. Cui and P. K. Shen, *Carbon*, 2011, **49**, 3972-3982.

54. Y. Qiu, W. Li, W. Zhao, G. Li, Y. Hou, M. Liu, L. Zhou, F. Ye, H. Li, Z. Wei, S. Yang, W. Duan, Y. Ye, J. Guo and Y. Zhang, *Nano Letters*, 2014, **14**, 4821-4827.

55. C. Jin, W. Zhang, Z. Zhuang, J. Wang, H. Huang, Y. Gan, Y. Xia, C. Liang, J. Zhang and X. Tao, *Journal of Materials Chemistry A*, 2017, **5**, 632-640.

56. J. Zhang, H. Hu, Z. Li and X. W. Lou, *Angewandte chemie international edition*, 2016, **55**, 3982-3986.

57. Q. Pang and L. F. Nazar, *ACS Nano*, 2016, **10**, 4111-4118.

58. G. Zhou, Y. Zhao and A. Manthiram, *Advanced Energy Materials*, 2015, **5**, 1402263.

59. L. Qie and A. Manthiram, *Chemical Communications*, 2016, **52**, 10964-10967.

Table of Content

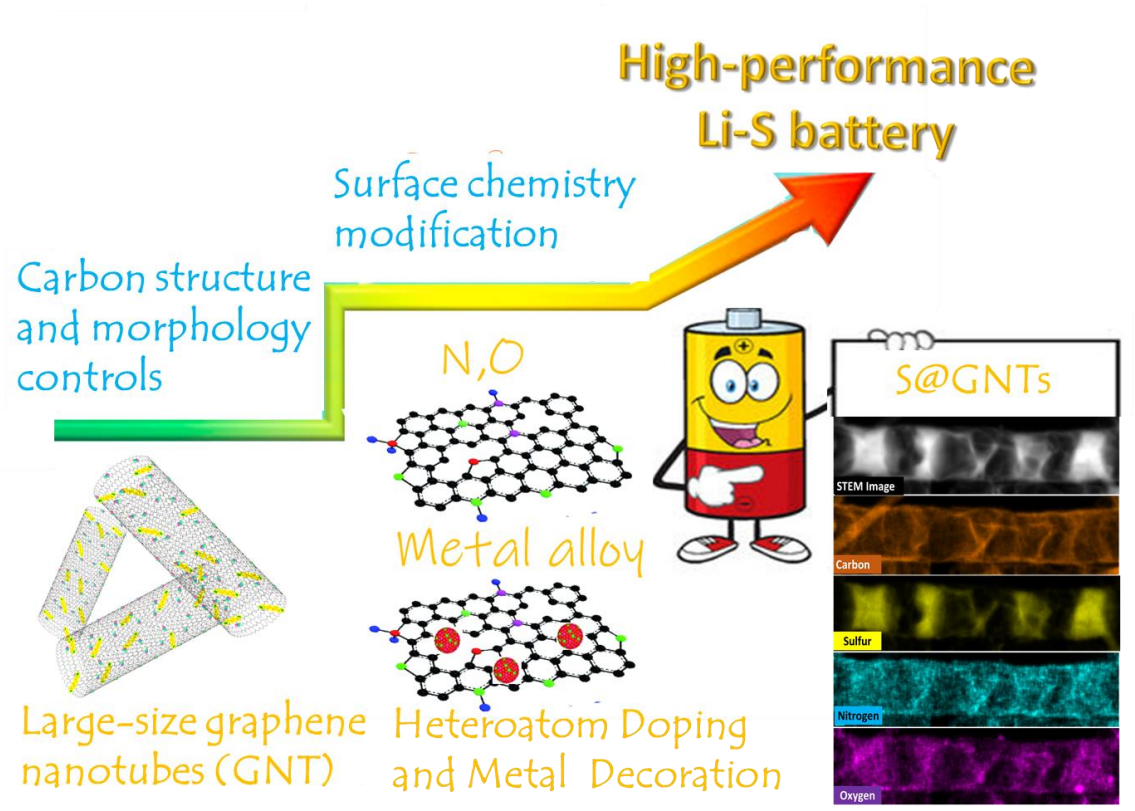

A large-size and heteroatom doped graphene tube host in S cathodes exhibited encouraging rate performance and cyclic stability for Li-S batteries.